Chapter 5

Dynamic Response of Micro-architectured VACNT Foams[4]

In this chapter, we present the design, fabrication, and dynamic characterization of micro-patterned vertically aligned carbon nanotube (VACNT) foams. The foams' synthesis combines photolithographic techniques with chemical vapor deposition to create materials with an effective density up to five times lower than that of bulk VACNT foams. We characterize their dynamic response performing impact tests at different strain rates. Results show that the dynamic stress-strain behavior of the micro-patterned foams is governed by the patterns' geometry and has negligible dependence on their bulk density. The energy absorption of the micro-patterned foams is higher than most other energy absorbing materials, such as honeycombs, foams, and composites of comparable density. Highly organized CNT microstructures can be employed as lightweight material for protective applications.

5.1 Introduction

Understanding the structure-property relationship in ordered, multiscale, structured materials is essential to design and create new materials with tunable bulk properties [170]. Nature offers abundant examples in which the choice of specific hierarchical organizations and constituent geometries leads to materials that optimally combine strength, toughness and stiffness [3]. These biological materials have been inspiring the design and fabrication of synthetic micro- and nano-structured materials with novel mechanical behaviors [2]. Synthetic cellular materials, such as honeycombs and open/closed cell foams, are widely used in structural applications due to their light weights and high strengths [147]. Compared to conventional foams, architected materials (also referred to as "mechanical metamaterials") allow for the reduction of the cell size

[4] This work was performed in collaboration with L. Lattanzi, who designed and synthesized the samples, and provided support for the dynamic characterization, analysis and writing of the findings.

down to the nano-scale and can be engineered in ordered arrays and geometries [2]. The control of structural architectures at different length scales allows the fabrication of materials with novel properties [2]. For example, introducing order and hierarchy in metallic microlattices improved their mechanical properties significantly, while maintaining very low densities (~ $9x10^{-4}$ g cm^{-3}) [171]. This was achieved by designing their microstructure in a periodic array of hollow tubes forming an octahedral unit cell, with feature sizes ranging from nanometer to millimeter [171]. Using hierarchical design principles, similar three-dimensional hollow ceramic nanostructures have been fabricated and shown to combine light weight with high damage-tolerance [172]. The structural design at different lengthscales also improves the energy absorption capability that is critical for protective materials [173].

The effect of structural hierarchy on the resultant bulk material properties has also been studied for carbon nanotube structures [51]. CNT foams provide a broad design space to engineer structures at the nano- and micro-scales that can influence the bulk mechanical properties. As such, CNTs can serve as model materials for the study of the fundamental rules for the structure-property relations that govern the mechanical responses. The compressive behavior of vertically aligned carbon nanotube forests under quasistatic conditions has been extensively studied [37,51,144], and reported a foam-like response with almost full recovery of large deformations. Because of their high compressive strength (peak stress), their high energy-absorption, and their low densities, vertically aligned CNT forests have been suggested as vibration damping layers [68] or shock and impact absorbers for electronics and space applications [69].

In an earlier work, we studied the effects of micro-structural organization on the quasi-static mechanical response of CNT foams [51]. We designed and fabricated micro-patterned CNT foams composed of different 2-D lattices: circles, lines, and concentric rings. Quasistatic compression tests of those structures showed that the patterning geometry played a fundamental role in determining the foam's bulk energy absorption, peak stress and recovery from deformation. Selected micro-pattern geometries lead to the fabrication of lighter materials, which preserve the mechanical response of the bulk CNT foams [51]. Light weight materials having high-energy absorption are widely studied for

space and transport industry applications, in order to improve safety and fuel economy [174]. Despite extensive studies on the mechanics of CNT-foams, the dynamic response of these materials has not been fully characterized. In particular, understanding their deformation modes and energy dissipation mechanisms during impact is important in order to build reliable and robust structures usable in applications. Here, we describe the impact response of micro-patterned CNT foams in order to characterize their high-rate deformation and their energy absorption capability. We show how the micro-structural geometries influence the stress-strain response and the impact performance.

5.2 Materials and methods

VACNT structures were grown on patterned silicon wafers using a floating catalyst thermal chemical vapor deposition (tCVD) process, as described in Section 2.1.1. The micro-patterns on the substrate (Figure 5.1.) were realized using photolithographic techniques described in Section 2.1.4. The fabricated samples had a cross sectional area of 20.63±6 mm^2 and a thickness of ~727±300 μm. The pattern's geometry determines the effective bulk density of the microstructures, which was obtained by dividing the measured weight by the sample's volume.

To characterize their mechanical behavior, both quasi-static and dynamic compression tests were carried out on all samples. The quasi-static tests were performed using an *Instron E3000 electropulse* testing system (see Section 2.3), at a constant strain rate of 0.03 s^{-1} and up to a maximum compressive strain of 0.25. The energy absorption was computed by calculating the area within the hysteresis loop in the stress–strain curve. The impact tests were performed on the dynamic testing set up described in Section 2.4. The patterned CNT foams, still attached to the silicon substrates, were glued to the flat-plunge striker using a double-sided copper tape on the substrate side. The striker was launched on a frictionless guide using a pneumatic cylinder, such that the VACNT specimens directly impacted the force sensor. A quartz impact force sensor (*PCB Piezotronics*) recorded the transient force-time history during impact. A high-speed camera (*Vision Research's Phantom V1610*) coupled to a microscopic lens (*Infinity*) and operated at 100,000 frames per second was used for *in-situ* visualization of the microscale dynamic

deformation during the impact. The dynamic displacement-time history was obtained by post processing the high-speed image sequence using commercial digital image correlation software (*Image System's TEMA*). The recorded dynamic displacement- and force-time histories were then used to obtain the dynamic stress-strain response of the CNT foams subjected to impact loading. To study rate effects, we used two different impact velocities, 0.95 m s^{-1} and 2.56 m s^{-1}.

From the dynamic constitutive (stress-strain) response obtained, we extracted several material properties such as loading modulus, peak stress, maximum deformation, energy dissipation, cushion factor, and percentage recovery (see Section 3.2.4 for definition of these parameters). The loading modulus was obtained by examining the initial slope of the stress-strain curve, while the energy dissipated was calculated by integrating the area of the hysteresis loop of each loading cycle. The dynamic cushion factor (C_{dyn}) was obtained from Equation 3.7. High-speed imaging of micro-scale deformation provides insights into the fundamental deformation mechanisms involved in different length- and time-scales.

To evaluate the rate sensitivity of the energy dissipation, the specific damping capacity (D) was calculated for the patterns made by concentric rings (Equations 5.1-5.3).

$$D = \Delta U/U \tag{5.1}$$

$$\Delta U = \oint \sigma d\varepsilon \tag{5.2}$$

$$U = \int_0^{\sigma_{max}} \sigma d\varepsilon \tag{5.3}$$

Here, ΔU is the dissipated energy (Equation 5.2), U is the energy absorbed (Equation 5.3), σ is the stress and ε the strain. To compare the energy absorption capabilities and the influence of the effective density measured in CNT structures with different pattern geometries, the specific energy absorption (SEA) was calculated by dividing the total energy absorbed up to the peak stress by the mass (m) of the specimen (Equation 5.4):

$$SEA = \frac{\int_0^{\sigma_{max}} \sigma d\varepsilon}{m} \quad . \tag{5.4}$$

5.3 Results and discussion

To study the role of different pattern geometries on the impact response of CNT structures we fabricated seven different micro-patterned VACNT foams, classified as: 1-D, 2-D periodic, and complex structures (Figure 5.1). Loading modulus, peak stress, maximum deformation (strain), and energy dissipation calculated from the dynamic stress-strain curves for all the seven VACNT foams tested are summarized in Table 5.1. We also used a 'control' VACNT foam sample for comparison. All these material parameters correspond to an impact velocity of 0.95 m s^{-1}.

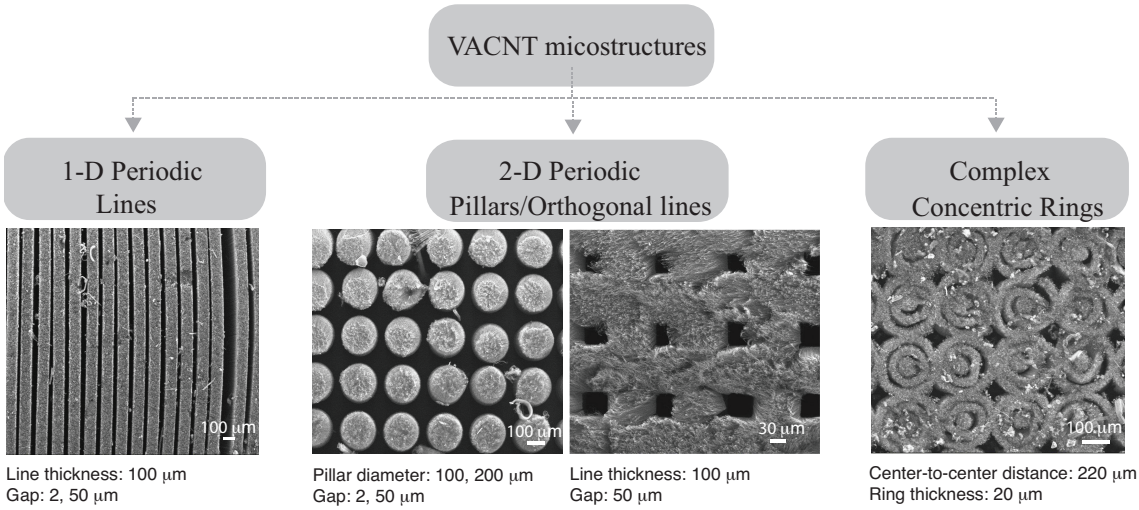

Figure 5.1. Schematic diagram and SEM images of the different VACNT microstructures, and the respective structural dimensions.

Table 5.1. Mechanical properties of the samples tested at an impact velocity of 0.95 m s^{-1}.

Specimen	Effective Density (g cm^{-3})	Energy Dissipation (MJ m^{-3})	Peak Stress (MPa)	Max Strain	Loading Modulus (MPa)	SEA (kJ kg^{-1})
VACNT forest	0.24	0.137	3.36	0.22	4.4	1.175
Lines 100; gap 2 μm	0.1 ± 0.03	0.085±0.014	0.59±0.08	0.36±0.04	1.1±0.12	1.103±0.
Lines 100; gap 50 μm	0.045 ± 0.02	0.17±0.05	0.95±0.09	0.52±0.06	1.42±0.03	4.35±1.9
Orthogonal lines	0.0716 ± 0.03	0.15±0.04	0.95±0.2	0.45±0.02	1.3±0.3	2.4±1.2
Pillars 100; gap 2 μm	0.08 ± 0.02	0.14±0.03	0.84±0.2	0.40±0.11	1.39±0.47	2.58±0.3
Pillars 100; gap 50 μm	0.0324 ± 0.02	0.14±0.05	0.53±0.07	0.48±0.02	1.14±0.6	7.4±4
Pillars 200; gap 50 μm	0.19 ± 0.05	0.18±0.03	1.11±0.05	0.46±0.05	1.36±0.5	1.11±0.2
Concentric rings	0.032 ± 0.02	0.11±0.01	1.26±0.06	0.26±0.14	5.9±2	4.59±2

Figure 5.2 (a) shows the dynamic mechanical response of both non-patterned (VACNT forest) and patterned (lines, pillars and concentric ring columns) structures impacted with a striker velocity of 0.95 m s^{-1}. The results clearly demonstrate that density plays a marginal role in determining the overall dynamic material response while the microstructural organization has a fundamental influence on the constitutive behavior. Despite their low effective density (0.032±0.02 g cm^{-3}), the structures composed of concentric ring columns exhibit the highest stiffness, with a compressive modulus of ~7 MPa. Such a modulus is higher than that of non-patterned VACNT structures (~4.4 MPa), which have an order-of-magnitude higher density (0.24 g cm^{-3}). As previously reported [41,51] the wide range of effective densities measured for both non-patterned and patterned structures depends on the synthesis process and on the position of the silicon wafer inside the furnace during growth. VACNT samples patterned with structures

having density values ranging from 0.08 to 0.19 g cm^{-3}—e.g., pillars with 100 μm diameters and 2 μm gaps, 100 μm thick lines separated by 2 μm gaps, and pillars with 200 μm diameters and 50 μm gaps, and orthogonal lines—undergo larger deformation than the samples patterned with concentric rings.

Results show that by changing the microstructural organization of CNTs it is possible to tune the stress-strain response. Despite having the same density (0.0324±0.02 g cm^{-3}), structures made of pillars with 100 μm diameters and 50 μm gaps exhibit a different mechanical behavior compared to that observed for the concentric ring columns, clearly demonstrating the fundamental role of geometry. The stress-strain curve measured for "pillars 100 gap 50" is characterized by an initial linear elastic regime, followed by a stress 'plateau' (Figure 5.2 (a)). Such foam-like behavior is also observed in patterns made by lines 100 μm thick separated by 50 μm gaps (0.045±0.02 g cm^{-3}). Interestingly, the plateau stress (σ_{pl}, defined as the average stress between 15% and 25% strain during compression) measured in samples patterned by lines is higher than that observed for pillars, measuring 0.31 MPa and 0.2 MPa, respectively.

As shown in Figure 5.2 (b), increasing the complexity of the structural architecture (from 1-D to 2-D periodic patterns) affects the stress-strain response. Up to $\varepsilon = 0.2$, the 1-D and 2-D periodic structures have the same stress-strain behavior. At higher strain values, the stress of the orthogonal line pattern increases steeply, while the 1-D structure shows a stress 'plateau' with positive slope. Importantly, the orthogonal lines exhibit a full recovery of the deformation. Figures 5.2 (a) and 5.2 (b) show that the stress-strain behavior of pillars and lines is affected by the gap values (varied between 50 μm and 2 μm). At an impact velocity of 0.95 m s^{-1} the pattern made of pillars with diameter of 100 μm and gap 2 μm reaches a strain of 0.3 and a peak stress of 1 MPa. In samples with patterns with a larger gap (50 μm), the strain and the peak stress are 0.45 and 0.48 MPa, respectively. Contrary to what is observed for patterns composed of pillars, the peak stress reached by lines with small gap (2 μm) is lower than the peak stress reached by lines with large gap values (50 μm).

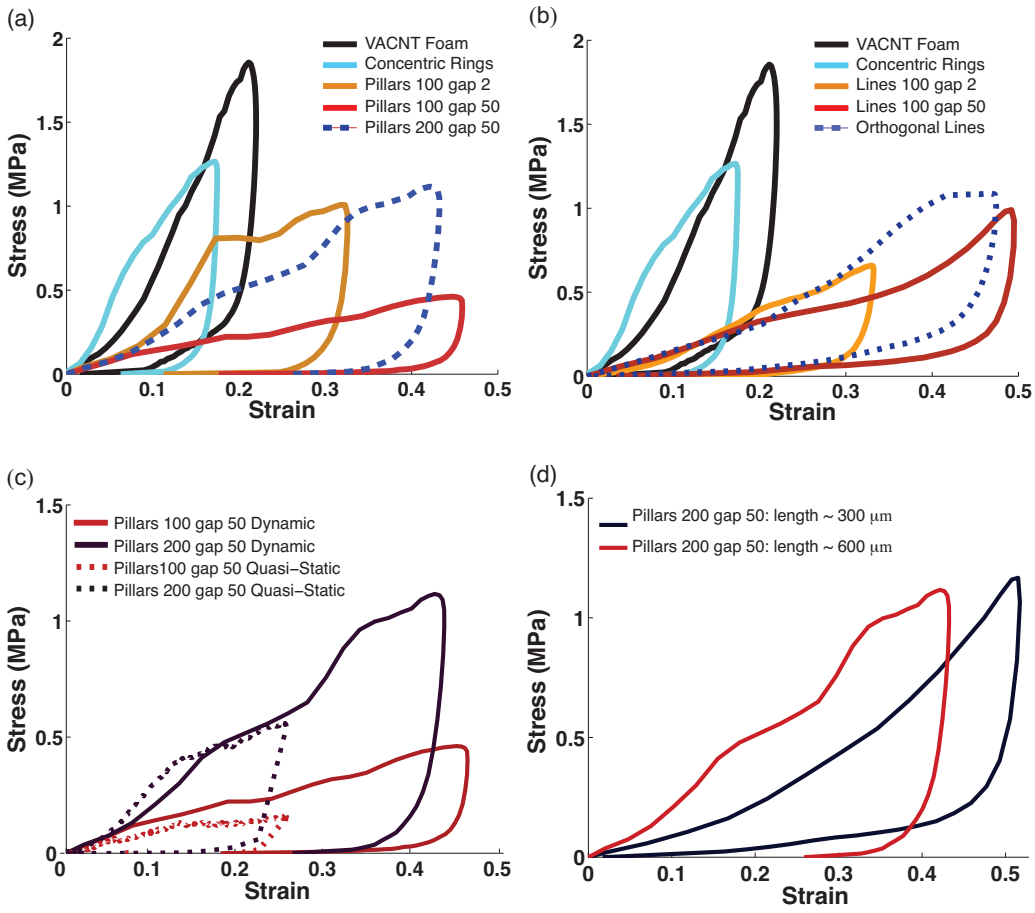

Figure 5.2. Stress-strain curves of VACNT samples patterned with different geometrical micro-architectures. **(a)** Response of patterns containing different pillars compared with bulk VACNT foams and with VACNT foams patterned with concentric rings. **(b)** Response of patterns containing different lines compared with bulk VACNT foams and with VACNT foams patterned with concentric rings. **(c)** Effect of variations of the pillar's diameter and **(d)** length on the quasi-static and dynamic response.

The role of the geometry on the hysteretic energy dissipation is also shown in Figures 5.2 (a) and 5.2 (b), and summarized in Table 5.1. The ability to dissipate energy (i.e., the area encircled by the hysteresis loop) improves in the micro-patterned VACNT samples compared to non-patterned VACNT forests. For example, by organizing VACNTs in pillars with diameters of 200 μm and gaps of 50 μm, the energy dissipation is increased up to ~1.7 times, and the peak stress decreases by ~3 times (compared to the same values

for bulk foams). Changing the gap size from 2 μm to 50 μm increases the energy dissipation by up to ~2 times, while the peak stress increases by ~1.3 times.

Figure 5.2 (c) shows the effect of the pillars' diameters on the quasistatic and dynamic mechanical response of the macrostructure. Both the peak stress and the energy dissipation increase as the pillar's diameter is increased (Figure 5.2 (c)). Under impact loading, the peak stresses reached by structures made of pillars with diameters of 200 μm and 100 μm measure 1.17 MPa and 0.45 MPa, respectively. The VACNT foams patterned with pillars with diameter of 200 μm dissipate 100% more energy than those structured with 100 μm diameter pillars. In quasistatic tests, the energy dissipated by pillars with larger diameters (6.8×10^6 J m^{-3}) is ~3 times higher than that measured for thinner pillars (2.1×10^6 J m^{-3}).

To control the sample's recovery, even after large deformations, we varied the length of the pillars (i.e., the overall thickness of the samples) by varying the precursor solution in the synthesis process, keeping all other parameters unchanged. 600 μm thick VACNT samples were fabricated using 25 ml of precursor solution and 300 μm thick samples were obtained with 15 ml of precursor solution. Testing results (Figure 5.2 (d)) show two main effects: (i) the slope of the initial segment of the stress-strain curve is significantly higher for longer pillars; (ii) upon unloading, the thinner samples (300 μm) show almost full recovery, while the 600 μm samples show lower recovery. The recoverability of VACNT arrays has been previously investigated and it is known to depend on the experimental testing setup, as well on the VACNT morphology [37,40,123,175]. A recent study [40] showed that the amount of precursor solution used, and hence the total reaction time, largely affects the morphology, the density and the alignment of VACNTs. The tortuosity, the diameter and the length of the CNTs were found to increase as a function of the growth time [40]. These properties reflected on the mechanical response and on the resilience of the structure. Since both the structures (300 μm and 600 μm long pillars) exhibit the same deformation mechanism, we hypothesize that the better recoverability of the thinner samples is related to the different morphology and distribution of the CNTs within the pillars, although this was not visible in the SEM images.

The effect of the microstructural organization on the fundamental deformation mechanisms of the CNT structures was also investigated using high-speed microscopy during and after the impacts. The *in-situ* images reveal that samples with a gap value of 2 μm, consisting of both pillars and lines, follow a uniaxial compression response. The high-speed image sequences suggest that the deformation initiates on the thin layer adjacent to the loading face (top of the CNT structure) and proceeds by sequential buckling at the opposite side of the microstructure (bottom of the CNT structure), a characteristic influence of the intrinsic density gradient in the VACNT structures [37]. Samples patterned with 50 μm gaps show a different microstructural deformation under impact tests compared to that observed in those with 2 μm gaps. When impacted, the pillars undergo lateral deflection without exhibiting sequential buckling at the low-density region (bottom). The deformation mechanism at the microscale might be compared to the buckling of an ideal column having one end fixed and the other end free to move laterally. The small lateral movements of the striker in the guide during impacts and the absence of lateral constraints at the force sensor-sample interface allow the top surfaces of the samples to slide laterally, while the opposite ends (the bottoms) are fixed to the silicon substrate. The results clearly show that the axial compressive impact force is higher than the critical load (or Euler buckling load) and it causes an inelastic, permanent deflection that does not recover after unloading. This behavior can also explain the low overall recovery observed in samples patterned with pillars spaced by larger gaps (50 μm). When the gaps are small (2 μm) the lateral deflection of the pillars is prevented by pillar-pillar interactions, which act as lateral supports and provide mechanical reinforcement.

However, even samples with equal gaps (50 μm) but different geometries (lines and pillars) deform differently. The 1-D organization of the lines and their high area moments of inertia result in large, global shear deformations (the lines are 100 μm thick, ~800 μm tall and ~4 mm long). Due to the gradient in density along the sample's thickness, an initially localized deformation (collective buckling) occurs at the bottom, low-density region of the samples. This initial non-affine deformation triggers a resulting shear deformation of the whole structure. Such large shear deformation is not observed in

patterns with 2 μm gaps, because of the mechanical constraint that occurs when the lines start buckling. The high-speed image sequences show that the diameter has also an effect on the overall response of VACNT samples patterned with pillars. Under impact, the pillars with diameters of 200 μm and gaps of 50 μm do not exhibit lateral deflection (as observed in pillars with 100 μm diameter), but they show uniaxial compression with the same characteristic sequential buckling as that observed in bulk CNT forests and in micro-patterned structures with small gap values. The critical buckling load of the individual pillars in the patterns depends on the "effective" elastic modulus of the materials from which they are composed, the pillar diameters, and their lengths. The increase of the pillar diameters increases the moment of inertia, hence providing the structures with a higher critical buckling load. In addition, the number of CNTs nodes (defined as sites of interaction between individual CNTs in a given structure) is higher in the micro-patterns made of pillars with diameters of 200 μm compared to the patterns made of pillars with diameters of 100 μm. This might explain the higher energy absorption capacity of the pillars with larger diameters. Whilst the pillars with diameters of 200 μm gaps of 50 μm increase substantially the peak stress and the energy absorption capacity compared to the pillars with diameters of 100 μm and gaps of 50 μm, they do not enhance the specific energy absorption (SEA).

Table 5.1 provides the SEA of the CNT foams patterned with different structures and tested with an impact velocity of 0.95 m s^{-1}. Results show that CNT foams organized in pillars with diameter of 100 μm and gap 50 μm have the highest specific energy absorbed, i.e., ~7.4±4 kJ kg^{-1}. Besides the high value of weight-specific energy absorption, such patterned structures show a constant plateau stress level (Figure 5.2 (a)), a desirable feature for an energy absorbing material.

The complex geometry of the micro-patterns made of columns of concentric tubes, allowed us to obtain lighter structures preserving the high mechanical response observed in the CNT bulk forest [51]. As previously reported [176–179], tubes are a common shape for energy absorption, in which energy can be dissipated in several modes of deformation. An understanding of the material behavior at high strain rates in terms of failure and energy absorption capability is essential for predicting the impact

performance of CNT structures patterned with columns of concentric tubes (Figure 5.3). The measured constitutive responses of these foams tested under different impact velocities are shown in Figure 5.3 (a). Figure 5.3 (b) and Figure 5.3 (c), which report selected image sequences acquired by the high-speed camera showing the buckling behavior of the columns, at different strain-rates.

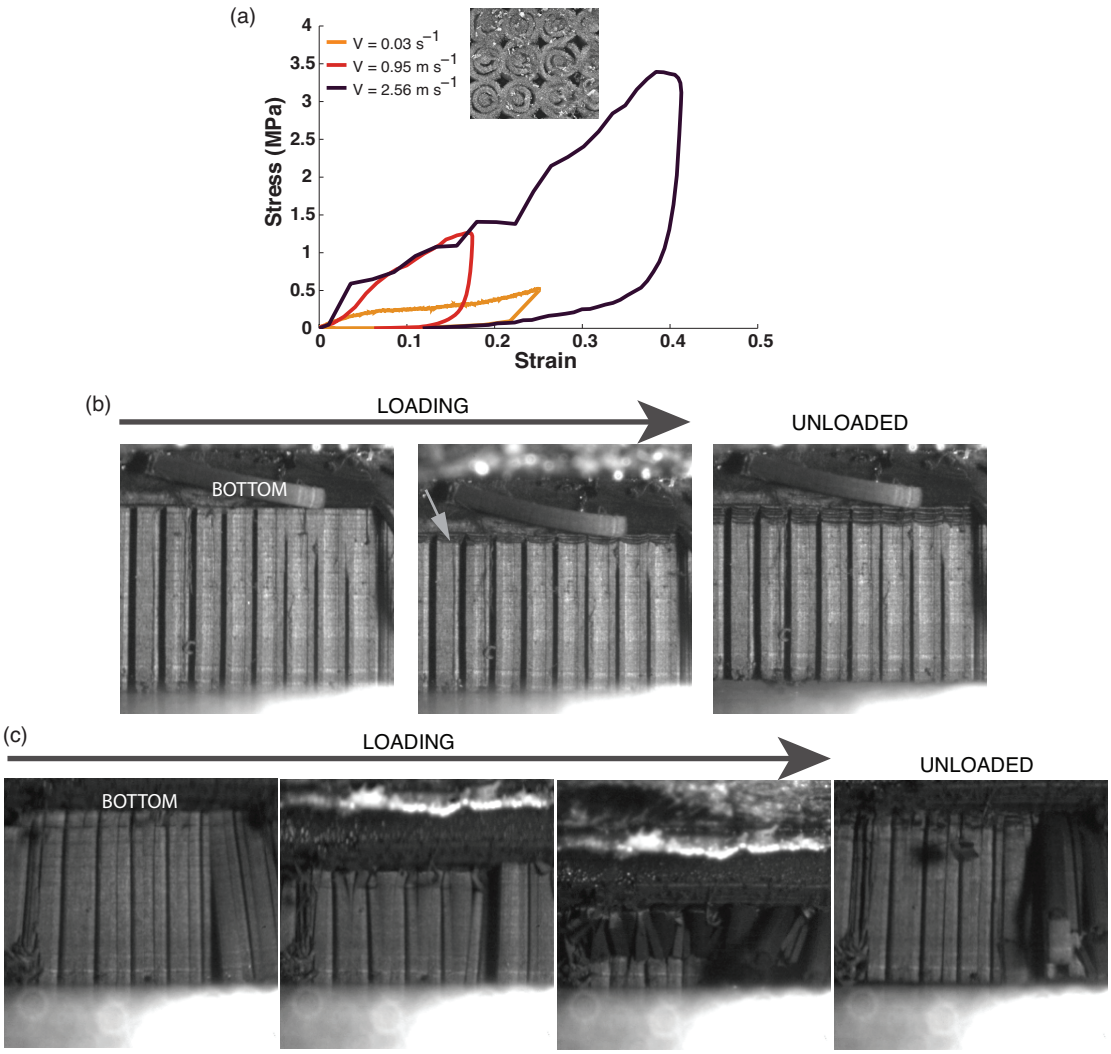

Figure 5.3. (a) Stress-strain curves of concentric rings at different strain rates. Deformation mechanism of concentric rings at the impact velocity of **(b)** 0.95 m s^{-1} and **(c)** 2.56 m s^{-1}.

Quasistatic tests, carried out at a strain rate of 0.03 s^{-1} (Figure 5.3 (a)) show an initial elastic region up to ~2.5% strain, followed by a long plateau region. Dynamic tests at

impact velocities of 0.95 m s^{-1} and 2.56 m s^{-1} show a different stress-strain behavior, exhibiting an increase in the measured stress. For example, the plateau stress reached by concentric rings under impact tests is significantly higher than the plateau stress measured in quasistatic tests. At high impact velocity (2.56 m s^{-1}), the concentric rings dissipate 0.6 MJ m^{-3}, while at 0.95 m s^{-1} the energy dissipated is 0.1 MJ m^{-3}. The specific damping capacity measured at the same impact velocities is compared with the quasistatic data. At impact velocities of 0.95 m s^{-1} and 2.56 m s^{-1}, the specific damping capacity of the samples patterned with concentric rings measures 0.9, while it is 0.5 for the quasi-static tests. The lower specific damping capacity measured in quasi-static, compared with the dynamic results, suggests strain-rate sensitivity in the materials' responses.

Figures 5.3 (b) and 5.3 (c) report *in-situ* experimental observations of the buckling of foams patterned with concentric tubes, under dynamic loading conditions. Despite the different stress-strain responses, the concentric tubes under quasistatic and dynamic loads (0.95 m s^{-1}) always collapse, forming progressive buckles, which develop at the bottom of the structure (in the low density region of the VACNTs), as shown in Figure 5.3 (b). The buckling observed is permanent, as the folds do not recover when unloaded. This suggests that at the impact velocity of 0.95 m s^{-1} the buckling is still driven by the nanostructure (the aligned CNTs of the column collapse into folds).

The high-speed image sequence of the microstructure at different stages of crushing shows that at the higher impact velocity, 2.56 m s^{-1}, the columns exhibit a much larger deformation and a global buckling mode (Figure 5.3 (c)). This suggests that at the highest impact velocity the buckling is driven by the microstructural geometry, as opposed to that of the nanostructure (CNT density and entanglement). The buckling starts close to the low-density region (bottom) of the column in a fold with a wavelength higher than that observed in columns impacted at lower impact velocity. As compression progresses, a second fold develops just next to the first one. With further compression, the strain localizes close to the mid-height of the column, causing a global structural buckling of the columns. Interestingly, despite the pronounced buckling, the columns recover ~75% of their original shape.

To study the impact absorption efficiency of the patterned VACNT microstructures, we calculated the dynamic cushion factor (C_{dyn}) and plotted this value against the maximum strain (ε_{max}). The cushion factor as a function of the maximum strain was calculated for the impact velocities of 0.95 m s^{-1} and 2.56 m s^{-1}, shown in Figures 5.4 (a) and 5.4 (b), respectively. Both an increase in energy absorption and decrease in the peak stress contribute to decrease the cushion factor, which is desirable for impact protection. At the lower impact velocity (0.95 m s^{-1}), VACNT foams patterned with 1-D and 2-D periodic arrays exhibit improved cushioning (Figure 5.4 (a)).

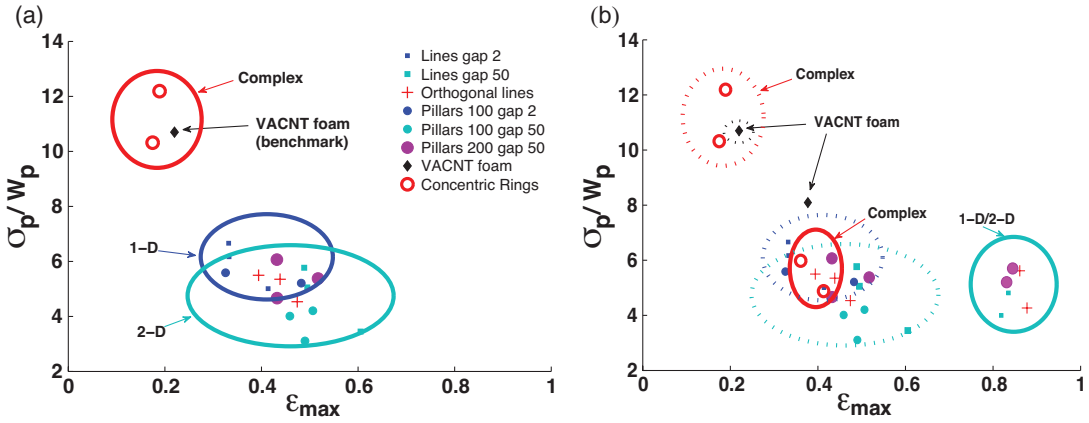

Figure 5.4. Plot of the cushion factor (σ_p/W_p) as a function of the maximum strain (ε_{max}) for patterned and non-patterned structures at impact velocities of **(a)** 0.95 m s^{-1} and **(b)** 2.56 m s^{-1}.

Compared to non-patterned VACNT forest samples, the line arrays (1D) and pillars and orthogonal-line arrays (2D) deform more at moderate stress levels. The increased energy absorption due to the large deformations at moderate stress-levels contributes to a reduction in the cushion factors. In contrast, the complex structure of concentric rings exhibits a higher cushion factor due to lower deformation and higher peak stress reached during testing. However, the cushioning performance of concentric ring columns exhibit the best performance at higher impact velocity (2.56 m s^{-1}), whereas the other samples of 1-D and 2-D arrays of lines and pillars reached their performance limit, deforming beyond the densification strain (Figure 5.4 (b)). It should be noted that the concentric ring columns deformed only 40% at 2.56 m s^{-1} and have the capacity to cushion much higher

velocities of impacts. In Figure 5.5, we compare the specific energy absorption of the patterned VACNT foams, impacted at the velocity of 2.65 m s^{-1}, to that of existing impact absorbing materials at full compaction (i.e. metal/polymer cellular structures [180], sandwiches [181], and tubes [182–184]).

At high impact velocity, the VACNT foams patterned with concentric rings have a more competitive SEA than existing energy absorber materials. The syntactic foams based on an aluminum matrix [185] and the polymer foams reinforced with small carbon fiber reinforced epoxy tubes [182] outperform the CNT concentric rings, however the high specific energy absorption correlates to higher values of their density (Figure 5.5).

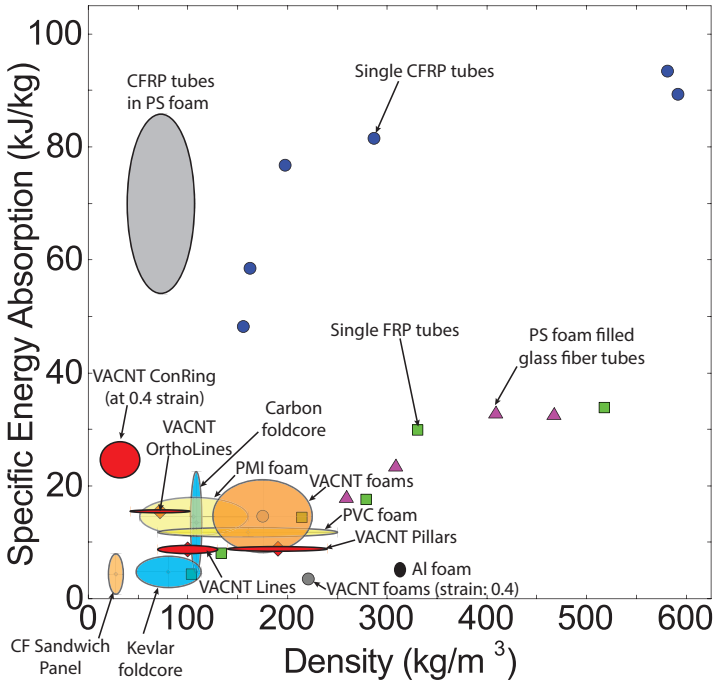

Figure 5.5. Specific energy absorption (SEA) values of VACNT microstructures and other existing impact absorber materials.

It is important to note that, in contrast to all other structures, the SEA of VACNT foams patterned with concentric rings is measured at the maximum strain of 0.4, and not during their full compaction. In addition, the *in-situ* videos reveal their almost full recovery and the absence of permanent damage, whereas all other materials/structures in Figure 5.5

undergo permanent failure. The results show that the SEA is strongly dependent on the microstructural organization of the VACNT foams and on the impact velocity. Finally, the results demonstrate that variations in the geometry of the micro-architectures can be used to control the impact performance of CNT foams in a broad design space, which can be made to address specific applications. Such extremely lightweight materials, characterized by high stiffness, strength, and energy absorption capacities, are very attractive for weight sensitive applications (i.e. automotive and aerospace applications).

5.4 Conclusions

We present the fabrication and the bulk dynamic characterization of new foam materials consisting of micro-patterned VACNT forests. The patterning results in materials with significantly reduced bulk density (up to 20 times lower than non-patterned VACNT foams), but with similar, or up to an order of magnitude improved, dynamic performance (considering peak stress and energy absorption capacity). The geometry of the micro-structural architectures and the impact velocity (loading rate) largely affect the deformation mechanisms and the bulk stress-strain response of these materials. In particular, changes in the microscale geometry of the patterns allowed the tuning of the specific energy absorption (SEA) of VACNTs under impact loading. By organizing VACNTs in concentric ring columns, for example, we obtained a value of SEA >25 kJ kg^{-1} that is competitive with that of existing energy absorbers described in literature. The patterned VACNT foams described in this work hold great potential for application as novel lightweight materials for impact protection.